ChemPubSoc Europe

DOI: 10.1002/ejic.201700240

EurJIC European Journal of Inorganic Chemistry

Full Paper

Eu-Based Bioprobes

Amine-Functionalized Silica Nanoparticles Incorporating Covalently Linked Visible-Light-Excitable Eu^{3+} Complexes: Synthesis, Characterization, and Cell-Uptake Studies

Biju Francis,[a,b] Bernhard Neuhaus,[c] M. L. P. Reddy,*[a] Matthias Epple,[c] and Christoph Janiak*[b]

Abstract: We report the synthesis, characterization, photophysical investigations, and cell-uptake studies of luminescent silica nanoparticles incorporating covalently linked visible-light-excitable Eu^{3+} complexes. Visible-light excitation was accomplished by using highly conjugated carbazole-based β-diketonate ligands. Covalent incorporation of the Eu^{3+} complexes into the silica nanoparticles was achieved by modification of the bidentate phosphine oxide 4,6-bis(diphenylphosphoryl)-10*H*-phenoxazine (**DPOXPO**), which was used as the neutral donor for the Eu^{3+} ion. The surface amine functionalization of the nanoparticles was carried out using aminopropyltriethoxysilane (APTES). The prepared nanoparticles (**Eu@Si-OH** and **Eu@Si-NH2**) are around 35–40 nm in diameter, monodisperse, stable in aqueous dispersion, and also retain the luminescent properties of the incorporated Eu^{3+} complex. The synthesized nanoparticles exhibit a promising luminescence quantum yield of 38 % and an excited-state lifetime of 638 μs at physiological pH. The photobleaching experiments revealed that the developed nanoparticles are more photostable than the parent Eu^{3+} complex **1**. In vitro experiments with **Eu@Si-NH2** nanoparticles on HeLa cells showed that they are biocompatible and are readily taken up by cells.

Introduction

Luminescence-based imaging techniques have achieved great attention because of their high sensitivity, versatility and ease of usage in in-vitro as well as in in-vivo imaging experiments.[1–4] The limited optical qualities of organic dyes (weak photostability) and quantum dots (potential cytotoxicity, blinking of fluorescence and complex functionalization strategies) often limit their imaging possibilities and demand the development of better bioprobes.[5–8] Because of their appealing characteristics, such as high biocompatibility, chemical inertness, optical transparency, high water dispersibility, and easy surface-functionalization strategies, silica nanoparticles are an attractive platform for bioprobes.[9–11] Moreover, encapsulation into silica nanoparticles improves the chemical and photostabilities of the loaded species.[12–14] The remarkable optical properties of lanthanide ions (Ln^{3+}), such as narrow emission bands, high color purity, large Stokes shifts, and long luminescent decay times, have often been combined with the advantageous characteristics of silica nanoparticles.[15–19] However, the use of Ln^{3+} ions as bioprobes is restricted, due to their low molar-absorption coefficients and UV excitation wavelengths.[20–22] The development of visible-light-excitable Eu^{3+} antenna complexes, which avoid the harmful UV irradiation and possess high molar-absorption coefficients, augments their attractiveness in this scenario.[23–25] The drawback of poor water solubility of these complexes can be overcome by incorporating them into silica nanoparticles, which provide better water dispersibility.[26–28] Hence, the past decade has witnessed a surge in research for the development of luminescent silica nanoparticles, whose optical properties and biocompatibilities are promising for various biological applications, by incorporating visible-light-excitable Eu^{3+} complexes.[29–31]

Compared with other preparation methods, like impregnation and doping, covalent linking of dye molecules to silica nanoparticles reduces the risk of the dyes being leached out.[32–34] Furthermore, it improves the homogeneity of the nanoparticles and allows higher loading.[35] Previous works concerning the covalent attachment of Eu^{3+} complexes to the silica nanoparticles have been limited to the modification of primary ligands (β-diketonates or carboxylic acids)[36–38] or nitrogen-based neutral donors.[39–41] In comparison with nitrogen donor ligands like terpyridine, phenanthroline, etc., phosphine oxide molecules are much better neutral donors for Eu^{3+} ions.[42,43] The coordinating abilities and the charge transport properties of aromatic nitrogen-donor ligands like phenanthroline may be

[a] *CSIR-Network of Institutes for Solar Energy, National Institute for Interdisciplinary Science & Technology (NIIST), Thiruvananthapuram 695019, India*
E-mail: mlpreddy55@gmail.com
http://www.niist.res.in/english/
[b] *Institut für Anorganische Chemie 1, Universität Düsseldorf, Universitätsstr. 1, 40225 Düsseldorf, Germany*
E-mail: janiak@uni-duesseldorf.de
www.janiak.hhu.de
[c] *Inorganic Chemistry and Center for Nanointegration Duisburg-Essen (CeNIDE), University of Duisburg-Essen, Universitaetsstr. 5–7, 45117 Essen, Germany*
E-mail: matthias.epple@uni-due.de
www.uni-due.de/chemie/ak_epple/

Supporting information and ORCID(s) from the author(s) for this article are available on the WWW under https://doi.org/10.1002/ejic.201700240.

affected by the substituents on the ring, due to the involvement of the lone-pair electrons on N-atoms. However, this is not the case with phosphine oxide molecules, since the groups binding to phosphorus atoms have no influence on the coordinating ability of the phosphoryl oxygen atom.[44] Therefore, the modification of phosphine oxide ligands is more flexible, and easier, than the modification of nitrogen-donor ligands. In addition to this, bidentate phosphine oxide molecules form more rigid and stable complexes with Eu^{3+} ions, due to the strong Lewis acid–base interaction of the Eu^{3+} ion and the phosphoryl oxygen atom.[45] Even though there are a few reports where hybrid materials have been prepared by modifying monodentate phosphine oxide ligands, the use of modified bidentate phosphine oxides have rarely been explored.[46,47]

Herein, a novel bidentate phosphine oxide molecule, 4,6-bis(diphenylphosphoryl)-10*H*-phenoxazine (**DPOXPO**) (Scheme 1) was synthesized to be used as an efficient neutral donor for Eu^{3+} ions. Using our previously reported carbazole-based β-diketonate molecule as the primary ligand[48] and **DPOXPO** as the neutral donor, we prepared the corresponding Eu^{3+} complex **1** (Scheme 2) and investigated its photophysical properties. The newly designed **DPOXPO** has a functional NH group to which a variety of substituents can be introduced. We modified the **DPOXPO** by adding a substituted silyl group

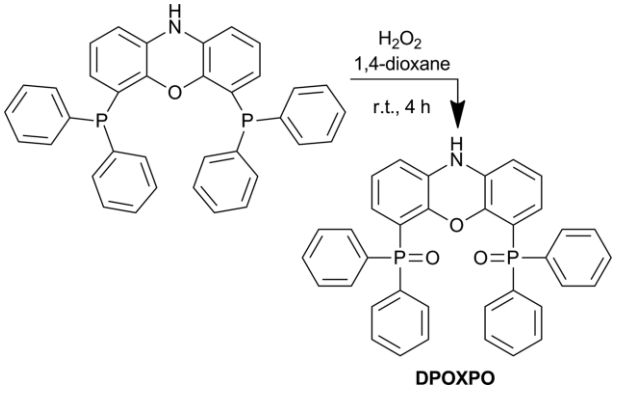

Scheme 1. Synthesis of the ligand **DPOXPO**.

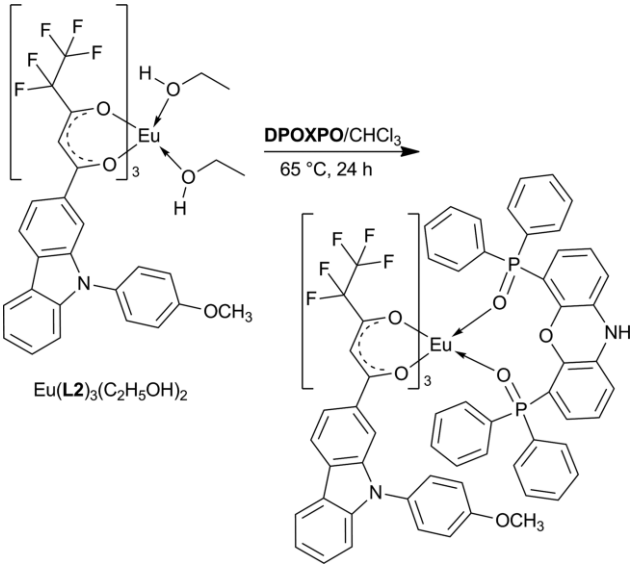

Scheme 2. Synthesis of Eu^{3+} complex **1**.

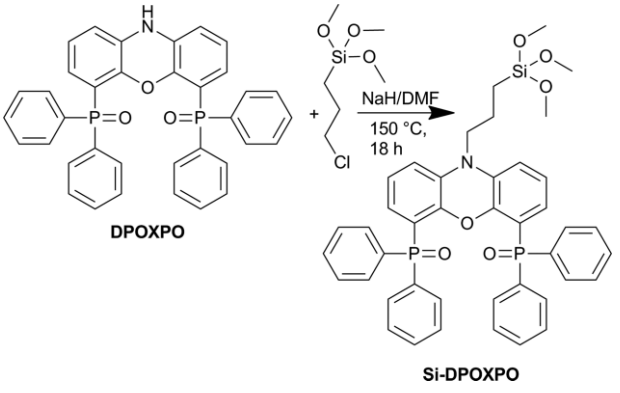

Scheme 3. Silylation of **DPOXPO**.

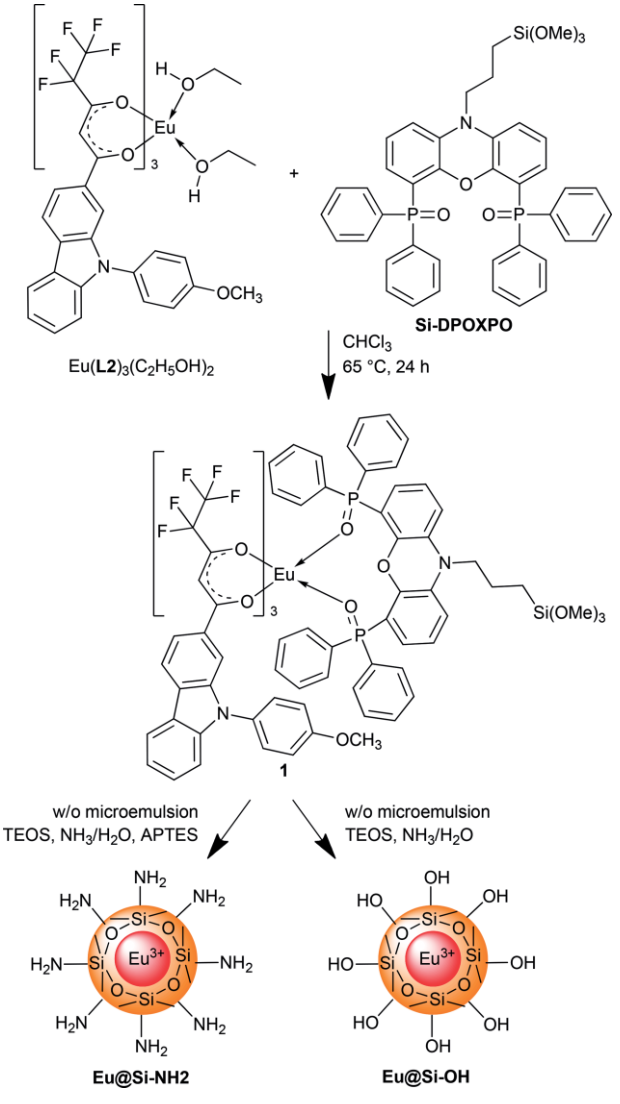

Scheme 4. Synthesis of **Eu@Si-NH2** and **Eu@Si-OH** nanoparticles. TEOS = tetraethyl orthosilicate, APTES = aminopropyltriethoxysilane.

(Scheme 3) and then covalently incorporated the resulting Eu^{3+} complex into silica nanoparticles (Scheme 4).

The amine functionalization of nanoparticles was done using aminopropyltriethoxysilane (APTES). The synthesized nanoparticles were characterized by FTIR spectroscopy, TEM, DLS spectrometry, and EDX spectroscopy. The surface amine functionalization was confirmed by ζ-potential measurements (in aqueous dispersions) and fluorescamine tests. The photophysical investigations suggest that the synthesized nanoparticles (**Eu@Si-OH** and **Eu@Si-NH2**) retain the excellent luminescence properties of the incorporated Eu^{3+} complexes. Photobleaching experiments of complex **1** and the nanoparticles reveal that the latter is more photostable than the former. The cell-culture studies on HeLa cells indicate that **Eu@Si-NH2** nanoparticles are taken up by the cells and are biocompatible.

Results and Discussion

Synthesis and Characterization of DPOXPO and Complex 1

The bidentate phosphine oxide ligand **DPOXPO** was synthesized as shown in Scheme 1 and was positively identified by ^{1}H, ^{13}C, and ^{31}P NMR spectroscopy, FTIR spectroscopy, and mass spectrometry, as well as by elemental analysis. The downfield shift observed in the ^{31}P NMR spectrum (from δ = –18.34 ppm to δ = 30.85 ppm) of **DPOXPO** confirms the successful oxidation of the phosphine to the phosphine oxide. The solvated complex, $Eu(\mathbf{L2})_3(C_2H_5OH)_2$ {H**L2** = 4,4,5,5,5-pentafluoro-3-hydroxy-1-[9-(4-methoxyphenyl)-9*H*-carbazol-2-yl]pent-2-en-1-one}, was synthesized according to the method described in our recent publication.[48] The synthesis procedure for Eu^{3+} complex **1** is depicted in Scheme 2. The synthesized complex was characterized using ^{31}P NMR spectroscopy, FTIR spectroscopy, ESI-MS methods, and elemental analysis. The ESI-MS and elemental analysis data indicated that the **DPOXPO** molecule replaces the solvent molecules in the coordination sphere of the Eu^{3+} ion. In the FTIR spectra, the P=O stretching frequency of the free **DPOXPO** ligand shifts from 1193 to 1144 cm^{-1} in complex **1**, which confirms the coordination of **DPOXPO** to the Eu^{3+} ion. This has been further confirmed by the upfield shift of the P=O signal (from δ = 30.85 ppm to δ = –91.90 ppm) in the ^{31}P NMR spectrum of complex **1**.

Synthesis and Characterization of Silylated DPOXPO and Eu^{3+} Conjugate [$Eu(L2)_3$(Si-DPOXPO)]

The silylation of the bidentate phosphine oxide ligand was done according to the synthetic route outlined in Scheme 3. The silylated ligand (**Si-DPOXPO**) was characterized using ^{1}H, ^{13}C, ^{31}P, and ^{29}Si NMR spectroscopy and FTIR spectroscopy, as well as elemental analysis. Similar to **DPOXPO**, the peak corresponding to the P=O resonance appears at δ = 31.03 ppm in the ^{31}P NMR spectrum. In the ^{29}Si NMR spectrum (Figure S1), the presence of a peak at δ = 42.9 ppm indicates the successful silylation of **DPOXPO**. In the FTIR spectrum, the band corresponding to the P=O stretching appears at 1193 cm^{-1}. The elemental analysis further confirms the successful silylation of **DPOXPO**. Using **Si-DPOXPO** as a neutral donor, we synthesized the corresponding Eu^{3+} complex [$Eu(\mathbf{L2})_3$(**Si-DPOXPO**)] (**1**) and used it as the precursor for the synthesis of luminescent nanoparticles without further purification.

Synthesis and Characterization of Nanoparticles

To obtain a homogeneous dye distribution and better photostability, the dye molecule has to be covalently linked to the matrix.[35] Using the one-pot water-in-oil microemulsion method,[49] we have covalently incorporated the long-wavelength-excitable Eu^{3+} complex [$Eu(\mathbf{L2})_3$(**Si-DPOXPO**)] into silica nanoparticles, with TEOS as the precursor for silica-shell formation (Scheme 4). The addition of aqueous ammonia, which catalyzes the hydrolysis and condensation of TEOS onto the [$Eu(\mathbf{L2})_3$(**Si-DPOXPO**)] conjugate, led to the growth of the silica shell on [$Eu(\mathbf{L2})_3$(**Si-DPOXPO**)]. APTES was used to modify the surface of the nanoparticles with NH_2 groups. The synthesized nanoparticles were characterized using FTIR spectroscopy, DLS spectrometry, TEM, and EDX spectroscopy. In the FTIR spectra, the broad band at 3400 cm^{-1} corresponds to the OH and NH_2 groups present on the surface of the nanoparticles. The band at 1092 cm^{-1}, with a shoulder at 1210 cm^{-1}, can be assigned to the asymmetric vibration of the Si–O–Si group.[50] The characteristic symmetric vibration of Si–OH and the asymmetric vibration of the Si–O–Si groups are responsible for the bands observed at 800 and 952 cm^{-1}, respectively. The band at 467 cm^{-1}, due to the O–Si–O bending vibration, is also present in the FTIR spectrum of **Eu@Si-NH2** nanoparticles. The TEM images (Figures 1 and S2) indicate that the nanoparticles are monodispersed and have spherical morphology, with average particle sizes of 38 and 42 nm for the **Eu@Si-NH2** and **Eu@Si-OH** nanoparticles, respectively (ascertained by measuring 50 particles in each case). The hydrodynamic diameters of the nanoparticles determined by DLS spectroscopic measurements are found to be 65–70 nm, and this takes into account their motion and the solvent sphere around the particles (Figure S3). Comparing the integrated areas of the peaks corresponding to silicon and europium in energy-dispersive X-ray (EDX) spectroscopy (Figure S4), we have determined a silica/Eu^{3+} complex molar ratio of 1:0.01,

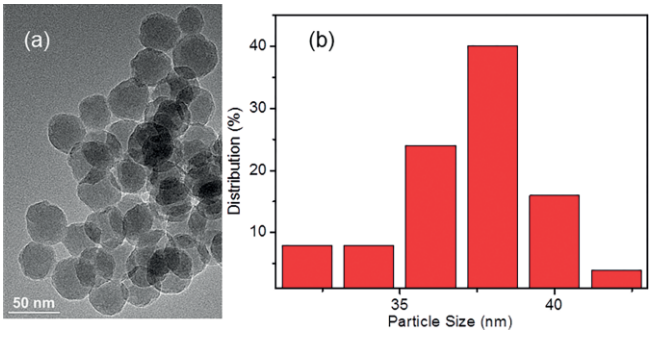

Figure 1. (a) TEM image (scale bar 50 nm) and (b) histogram depicting the diameter size distribution of **Eu@Si-NH2** nanoparticles. From the image contrast in (a), the individual nanoparticles could be clearly seen and their size determined, despite the aggregation and superimposition from the drying process during the TEM-grid preparation.

giving about 5500 Eu complexes per nanoparticle (see Supporting Information for estimate). The surface charge of the unmodified (**Eu@Si-OH**) and NH_2-functionalized (**Eu@Si-NH2**) nanoparticles was determined by measuring the respective ζ-potential values, –5.8 and +15.6 mV, after dispersion in pure water (i.e., at neutral pH), with the latter confirming the NH_2 functionalization (partial protonation of the amino groups at neutral pH). The NH_2 functionalization was further confirmed by the fluorescamine test, in which the **Eu@Si-NH2** nanoparticles showed a broad fluorescence signal, with a peak maximum around 480 nm (Figure S5) after the addition of fluorescamine.[51,52]

UV/Vis Absorption Spectra

The UV/Vis absorption spectra of the parent Eu^{3+} complex **1** (in chloroform solution) and the synthesized nanoparticles (in aqueous dispersion) are depicted in Figure S6. The absorption spectrum of complex **1** exhibits two distinct broad bands. The band with a maximum at around 360–400 nm corresponds to the electronic transitions of the enol moiety of the β-diketonate ligand, and the band in the higher energy region of 240–280 nm is attributable to the electronic transitions of the carbazole backbone.[53,54] The electronic transitions of the enol moiety of the β-diketonate ligand (band at ca. 310–400 nm) and the chelated phosphine oxide (band at ca. 300–380 nm) units are overlapped in complex **1**. The absorption spectra of the nanoparticles also display two broad bands, due to the electronic transitions of the enol moiety and carbazole ring of the β-diketonate ligands. Compared with complex **1**, the absorption bands of the nanoparticles (**Eu@Si-OH** and **Eu@Si-NH2**) are slightly redshifted, which may be due to the change in the environment of the Eu^{3+} complex within the nanoparticles. The scattering effect of the nanoparticles may also contribute towards the redshift of the absorption spectrum.

Photoluminescence Studies

The room-temperature excitation and emission spectra of complex **1** in chloroform solution and the nanoparticles in PBS buffer solution at pH 7.4 are recorded and given in Figure 2. From the excitation spectra, it is clear that the ligand excitation bands of the luminescent nanoparticles match well with the excitation spectra of the parent Eu^{3+} complex **1**. The absence of sharp Eu^{3+} ion absorption bands in the excitation spectra indicates that sensitization via ligand excited states is more efficient than the direct excitation. The emission spectra of complex **1** and the nanoparticles exhibit the characteristic emission bands of Eu^{3+} ions when excited at 400 nm (Figure 2).[55–57] The electric-dipole-induced hypersensitive $^5D_0 \rightarrow {}^7F_2$ transition is dominating in both cases, and it is responsible for the bright red color of complex **1** and the nanoparticles.[58] Visible-light excitation of the parent complex is retained in the developed nanoparticles, as demonstrated in Figure 2e, where the nanoparticles are excited by blue light. The absence of broad ligand emission bands in the emission spectra suggests that sensitization via ligand excited states is efficient.[59] The photophysical studies revealed that the synthesized nanoparticles retain the excellent luminescence properties of the incorporated Eu^{3+} complex.

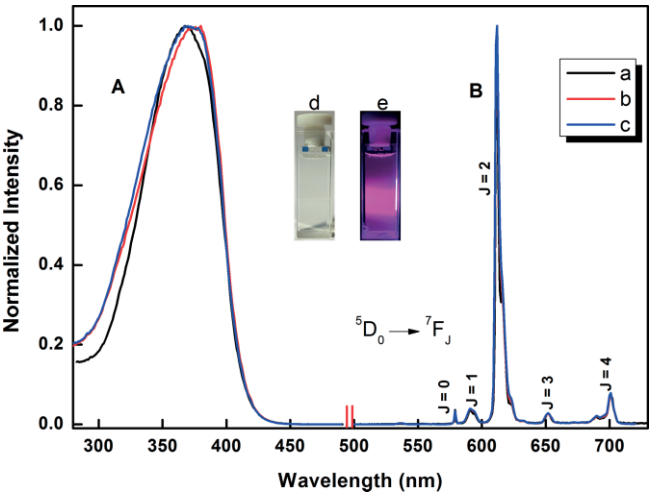

Figure 2. (A) Normalized excitation spectra (emission monitored at 612 nm) and (B) normalized emission spectra (excited at 400 nm) of: (a) complex **1** in chloroform solution, (b) **Eu@Si-NH2**, and (c) **Eu@Si-OH** nanoparticles dispersed in PBS solution (pH 7.4). In the normalized emission spectra (B), the spectra for (a), (b), and (c) are essentially superimposed. Photographs of the aqueous dispersion of **Eu@Si-NH2** nanoparticles under: (d) normal light and (e) blue light.

Photostability Studies

The photostabilities of the parent Eu^{3+} complex **1** and the prepared nanoparticles (**Eu@Si-NH2** and **Eu@Si-OH**) are shown in Figure 3. A chloroform solution of complex **1** and PBS dispersions of the nanoparticles were used for the studies. The intensity at 612 nm was monitored at 15 min time intervals under continuous exposure at 365 nm. After 4 h of continuous UV irradiation, broad ligand fluorescence dominated the emission

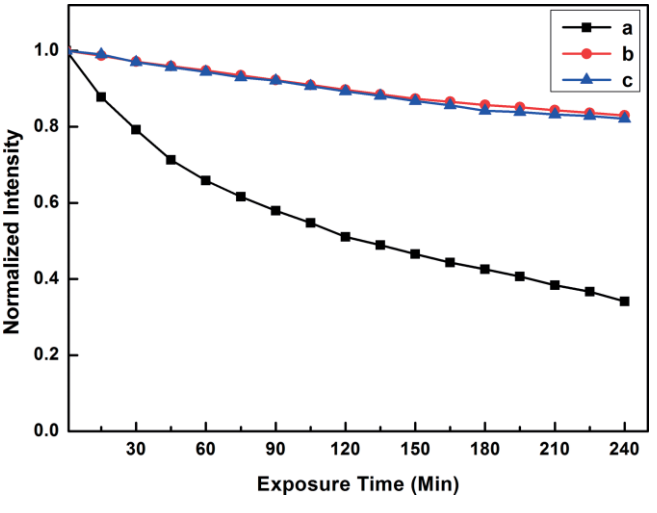

Figure 3. Photostability experiments of: (a) parent Eu^{3+} complex **1** in $CHCl_3$ solution, (b) **Eu@Si-NH2**, and (c) **Eu@Si-OH** nanoparticles dispersed in PBS buffer (pH 7.4) under continuous exposure at 365 nm. The luminescence intensity was monitored at 612 nm at 15 min intervals.

spectrum of the parent complex, which implies a complete decomposition of complex **1**. On the other hand, the photodecomposition of the nanoparticles **Eu@Si-OH** and **Eu@Si-NH2** is less than 15 %, even after 4 h of continuous UV irradiation. Here, the silica shell acts as a protective layer to the encapsulated Eu^{3+} complex in the nanoparticles and isolates the complex from the external environment. This clearly shows that by incorporation into the silica nanoparticles, the photostability of the dye molecules can be improved significantly.

Luminescence Decay Profiles

The antenna complexes of Eu^{3+} ions usually exhibit long luminescence lifetime values (µs to ms range).[57,60,61] The excited-state lifetimes of complex **1** in chloroform solution and the nanoparticles **Eu@Si-NH2** and **Eu@Si-OH** in PBS buffer solution at pH 7.4 were measured by monitoring the emission band at 612 nm when excited at 400 nm. The luminescence decay profile of the **Eu@Si-NH2** nanoparticles at room temperature is depicted in Figure 4, and those of complex **1** and the **Eu@Si-OH** nanoparticles are depicted in Figures S7 and S8, respectively. The single-exponential fitting of the decay curves in all compounds indicates the existence of a single coordination environment in complex **1** and in the developed nanoparticles. The excited-state lifetime of complex **1** was 719 ± 2 µs, whereas those of the **Eu@Si-NH2** and **Eu@Si-OH** nanoparticles were 537 ± 5 and 638 ± 5 µs, respectively (Table 1). The relatively shorter lifetimes observed for the nanoparticles may be due to the presence of OH and NH_2 groups, which activate the nonradiative decay pathways.

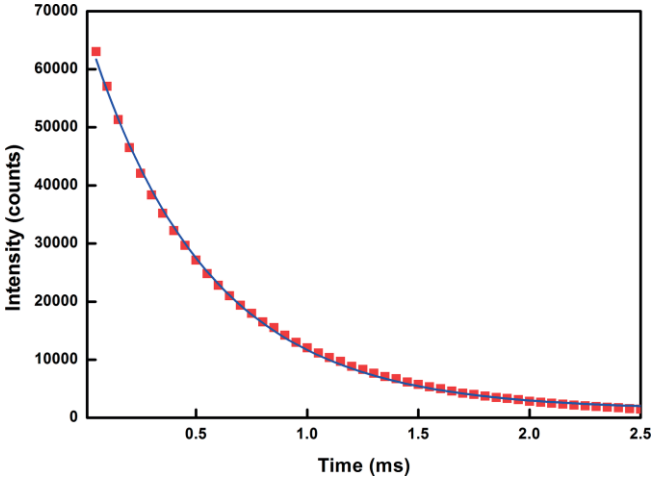

Figure 4. Luminescence lifetime profile of **Eu@Si-NH2** nanoparticles dispersed in PBS solution (pH 7.4) at room temperature (emission monitored at 612 nm).

Table 1. $^5D_0$ lifetime (τ_{obs}) and luminescence quantum yields (Φ) of complex **1** in $CHCl_3$ solution and **Eu@Si-NH2** and **Eu@Si-OH** nanoparticles in PBS dispersions.

Compound	τ_{obs} [µs]	Φ [%]
Complex **1**	719 ± 2	42
Eu@Si-OH	537 ± 5	38
Eu@Si-NH2	638 ± 5	34

The Eu^{3+} β-diketonate complexes are well known for their remarkable luminescence quantum yield values. Recently, an Eu^{3+} β-diketonate complex and its corresponding hybrid material were reported with quantum yield values of 82 % and 63 %, respectively.[61] In the present study, the luminescence quantum yield of the Eu^{3+} complex in chloroform solution is found to be 42 %. The incorporation of Eu^{3+} complexes into silica nanoparticles is usually unfavorable in the perspective of luminescence quantum yield. The nanoparticles **Eu@Si-NH2** and **Eu@Si-OH** were dispersed in PBS buffer at pH 7.4 and the luminescence quantum yields were estimated to be 34 % and 38 %, respectively (Table 1). The slight decrease in the quantum yields of the developed nanoparticles may be due to the increase in the nonradiative decay pathways associated with the high frequency oscillators (OH and NH_2 groups) present in the **Eu@Si-NH2** and **Eu@Si-OH** nanoparticles. The quantum yield values of the parent Eu^{3+} complex and the developed nanoparticles are comparable with the previously reported values.[57,61,62] This observation further confirms that, after incorporation into the nanoparticles, the Eu^{3+} complex maintains its optical properties.

The quantum yields and lifetimes of Eu^{3+}-based hybrid materials do not usually follow the same trend.[27,35,60,61] The lifetime is the inverse of the total deactivation rate, which, in turn, is the sum of the radiative and nonradiative rates. On the other hand, the quantum yield depends only on the radiative rate at which the excited level is depopulated. Therefore, the absence of correlation between the quantum yield and the lifetime does not represent a contradiction. In some cases, the luminescence parameters improve after incorporation into hybrid materials, whereas in other cases, the luminescence parameters decrease when compared with the pure complex. The exact mechanism has rarely been reported. In our case, the large number of surface OH and NH_2 groups decreases the quantum yield and lifetime values compared with those of the parent Eu^{3+} complex, but we cannot directly correlate the quantum yield and lifetime values of the nanoparticles. Also, notably, the estimated error for the quantum yield measurements is ±10 % (see Exp. Sect.).

Cell-Imaging and Cell-Viability Studies

The cell-uptake studies with the nanoparticles were carried out using the HeLa cell line. The high Stokes shift for the **Eu@Si-NH2** nanoparticles permitted the visualization of them, together with the red dye CellMask (sequential excitation at different wavelengths). The CLSM images indicated that both kinds of nanoparticles, that is, **Eu@Si-NH2** and **Eu@Si-OH** (to a lesser extent), attached to the cells and were subsequently taken up by the cells (Figures 5 and 6). Most of the particles were attached to the cell membrane after 4 h of incubation, probably due to the electrostatic interaction between the positively charged **Eu@Si-NH2** nanoparticles and the negatively charged cell membrane. By z-stacking, we confirmed that the particles had entered the cell (data not shown). By the MTT assay,[63] which monitors the mitochondrial activity, we determined the cell viability after incubation with nanoparticles (Figure 7). More than 80 % of the cells were viable after 4 h of

incubation with the nanoparticles, indicating good biological compatibility for potential biomedical applications.

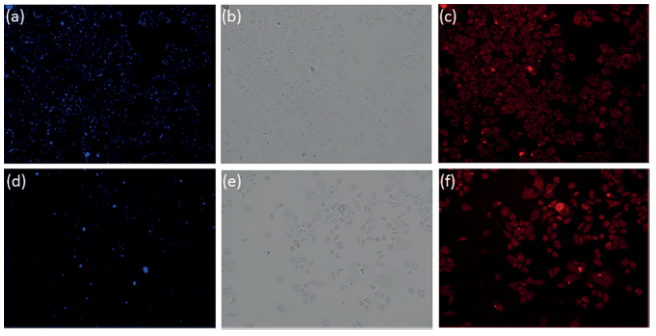

Figure 5. Pseudo-color images of HeLa cells incubated with **Eu@Si-NH2** nanoparticles [top row (a–c)], and **Eu@Si-OH** nanoparticles [bottom row (d–f)]. Images (a) and (d) show the fluorescent nanoparticles (artificial color in blue; original color red); (b) and (e) show bright field images of HeLa cells; (c) and (f) show the cell morphology stained with CellMask (red). All images were taken with a Keyence Biorevo BZ-9000 microscope. The cells were incubated for 4 h with the nanoparticles and were then thoroughly washed to remove dispersed and weakly adhering nanoparticles.

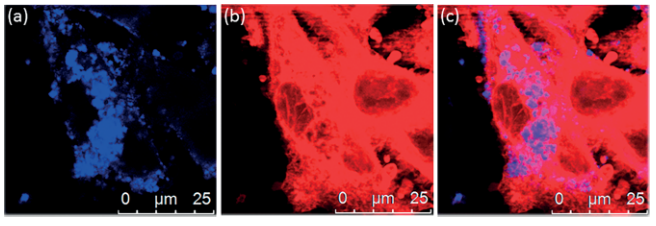

Figure 6. Magnified confocal-laser-scanning pseudo-color images of HeLa cells, incubated with **Eu@Si-NH2** nanoparticles: (a) artificially colored in blue [original luminescence color (red)], (b) stained with CellMask (red), and (c) a merged image. The cells were incubated for 4 h with the nanoparticles and were then thoroughly washed to remove dispersed and weakly adhering nanoparticles. The CLSM gives arbitrary colors, and to distinguish between red nanoparticles and red CellMask, we have colored them according to their excitation wavelengths (380 nm for the nanoparticles and 649 nm for CellMask).

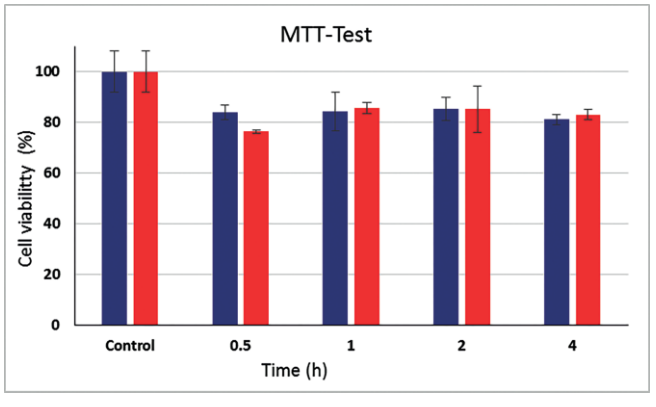

Figure 7. Viability (%) of HeLa cells assessed by the MTT assay. Untreated cells served as the control. All results are presented as the mean ± standard deviation (SD) from triplicate experiments. Blue bars correspond to the cell viability after treatment with **Eu@Si-OH** nanoparticles, and red bars correspond to the cell viability after treatment with **Eu@Si-NH2** nanoparticles. The cell viability is high in all cases.

Conclusion

We synthesized the visible-light-excitable, carbazole-based Eu^{3+} complex **1** using a novel bidentate phosphine oxide molecule **DPOXPO** as the neutral donor. The **DPOXPO** molecule has a functional NH group, and by modifying this group, we covalently incorporated the corresponding Eu^{3+} complex into silica nanoparticles. Amine functionalization of the nanoparticle surface was performed for biological studies. Synthesized nanoparticles were 35–40 nm in size, monodispersed, dispersible in water, and they retained the excellent luminescence properties of the incorporated Eu^{3+} complex. They exhibited a remarkable luminescence quantum yield, as high as 38 %, and an excited-state lifetime of up to 638 µs at physiological pH, both of which are comparable with the previously reported values. Photobleaching studies revealed that the synthesized nanoparticles were more photostable than the parent Eu^{3+} complex **1**. The cell-uptake studies with HeLa cells revealed that the amine-functionalized nanoparticles **Eu@Si-NH2** were taken up by the cells and were biocompatible. These interesting properties make the developed nanoparticles potential candidates for various biological applications. The large Stokes shift (excitation with blue light, emission of red light) makes them especially interesting as fluorescent probes that avoid interference with other staining reagents (like CellMask).

Experimental Section

General: Europium(III) nitrate pentahydrate, sodium hydride (60 % dispersion in mineral oil), aminopropyltriethoxysilane (APTES) and (3-chloropropyl)trimethoxysilane were procured from Sigma–Aldrich. Tetraethyl orthosilicate (TEOS) and Triton X-100 were purchased from Acros Organics. 4,6-Bis(diphenylphosphino)-10*H*-phenoxazine was obtained from Alfa Aesar. All other chemicals were of analytical reagent grade and used without further purification. Solvents were dried using standard methods. The solvated Eu^{3+} complex $[Eu(\mathbf{L2})_3(C_2H_5OH)_2]$ was synthesized according to the method described in our earlier publication.[48] The FTIR spectra of the compounds were measured using KBr pellets with a Bruker TENSOR 37 FTIR spectrometer, at ambient temperature, operating in the range 4000–500 cm^{-1}. A Bruker 500 MHz NMR spectrometer was used to record the ^{1}H (500 MHz), ^{13}C (125.7 MHz), ^{31}P (202.44 MHz), and ^{29}Si NMR (99.32 MHz) spectra of the newly synthesized compounds in [D]chloroform solution. C, H, and N elemental analyses were performed with a Perkin–Elmer Series 2 Elemental Analyzer 2400. A Thermo Scientific Exactive Benchtop LC/MS Orbitrap Mass Spectrometer was used to record the electrospray ionization (ESI) mass spectra. Dynamic-light-scattering spectrometry and zeta-potential determinations were performed with a Zetasizer Nanoseries instrument (Malvern Nano-ZS, laser: λ = 532 nm) using the Smoluchowski approximation; the data was taken from the Malvern software without further correction. The particle-size data refer to scattering intensity distributions (z-average). HR-TEM images and EDX spectra of the synthesized nanoparticles were collected with an FEI Tecnai G2 F20, with an acceleration voltage of 200 kV. The UV/Vis absorption spectra of the Eu^{3+} complex (in chloroform solution) and the nanoparticles (in aqueous dispersion) were recorded with a Shimadzu UV-2450 UV/Vis spectrophotometer, and the background correction of the spectra was made using the corresponding solvents. The photoluminescence (PL) spectra of the Eu^{3+} complex **1** (in chloroform solution) and nanoparticles (in PBS dispersion,

at pH 7.4), were recorded with a Spex-Fluorolog FL22 spectrofluorimeter equipped with a double grating 0.22 m Spex 1680 monochromator and a 450 W Xe lamp as the excitation source. The lifetime measurements of complex **1** (in chloroform solution) and the nanoparticles (in PBS dispersion, at pH 7.4) were carried out at room temperature using a Spex 1040 D phosphorimeter. The overall quantum yields for the parent Eu^{3+} complex and the developed nanoparticles were determined under ligand excitation (400 nm), based on the absolute method, using a calibrated integrating sphere in a Spex-Fluorolog spectrofluorimeter.[64] An Xe-arc lamp was used to excite the samples placed in the sphere, and the quantum yields were determined by comparing the spectral intensities of the lamp and the sample emission, as reported in the literature.[65,66] Using this experimental setup and the integrating sphere system, the solid-state and film-state fluorescence quantum yields of tris(8-hydroxyquinolinolato)aluminium (Alq_3) were determined to be 40 % and 18 %, respectively, which are consistent with previously reported values.[67,68] Each sample was measured several times under slightly different experimental conditions. The estimated error for the quantum yields is ± 10 %.[69,70]

Synthesis of 4,6-Bis(diphenylphosphoryl)-10*H*-phenoxazine (DPOXPO): 4,6-Bis(diphenylphosphino)-10*H*-phenoxazine (10 mmol) was dissolved in 1,4-dioxane (15 mL). H_2O_2 (2 mL, 30 %) was added dropwise to the solution, and the reaction mixture was then stirred at room temperature for 4 h. Water (10 mL) was then added to quench the reaction, and the solution was extracted with dichloromethane (3 × 20 mL). The organic layer was washed several times with water to remove excess 1,4-dioxane, dried with anhydrous Na_2SO_4, filtered, and the solvent evaporated. The product was obtained as an off-white powder (yield 99 %). $C_{36}H_{27}NO_3P_2$ (583.55): calcd. C 74.10, H 4.66, N 2.40; found C 73.96, H 4.49, N 2.42. ^1H NMR (500 MHz, $CDCl_3$): δ = 10.50 (br., NH), 7.20 (m, 22 H), 6.50 (m, 2 H), 5.98 (m, 2 H) ppm. ^{31}P NMR (202.44 MHz, $CDCl_3$): δ = 30.85 ppm. FTIR (KBr): $\tilde{\nu}_{max}$ = 3338 (br.), 1193 (P=O) cm^{-1}. MS: *m/z* = 584.1547 $[M + H]^+$.

Synthesis of Eu^{3+} Complex 1: The Eu^{3+} complex **1** was synthesized by stirring equimolar amounts of solvated complex $[Eu(\mathbf{L2})_3(C_2H_5OH)_2]$ and **DPOXPO** in chloroform solution at 65 °C for 24 h (Scheme 2). The solvent was then removed, and the product was purified by recrystallization from a chloroform/hexane mixture (15:85) (yield 76 %). ^{31}P NMR (202.44 MHz, $CDCl_3$): δ = –91.90 ppm. $C_{108}H_{78}EuF_{15}N_4O_{12}P_2$ (2122.68): calcd. C 61.11, H 3.70, N 2.64; found C 61.23, H 3.64, N 2.70. FTIR (KBr): $\tilde{\nu}_{max}$ = 3340 (br.), 3072, 1616, 1504, 1234, 1144 cm^{-1}. MS: *m/z* = 1660.2923 $(M - \mathbf{L2})^+$.

Synthesis of the Silylated Phosphine Oxide Si-DPOXPO: 4,6-Bis(diphenylphosphoryl)-10*H*-phenoxazine (1 mmol) was dissolved in dry DMF (10 mL) under N_2, with the temperature being maintained at 0 °C. Sodium hydride (2 mmol) was added, and the orange mixture was stirred for 2 h, while the reaction mixture was allowed to warm to room temperature. 3-Chloropropyltrimethoxysilane (1.9 mmol) was added dropwise at room temperature. The reaction mixture was then stirred at 150 °C for 18 h. After attaining room temperature, the yellow-brown suspension was filtered, and the solvent was removed under reduced pressure. The obtained product was then washed several times with hexane until an off-white powder was obtained (yield 72 %). $C_{42}H_{41}NO_6P_2Si$ (745.81): calcd. C 67.64, H 5.54, N 1.88; found C 67.86, H 5.72, N 1.64. ^1H NMR (500 MHz, $CDCl_3$): δ = 7.22 (m, 20 H), 6.66 (m, 2 H), 6.49 (m, 2 H), 5.97 (m, 2 H), 3.61 (s, 9 H), 3.49 (t, 2 H), 1.80 (m, 2 H), 0.72 (t, 2 H) ppm. ^{31}P NMR (202.44 MHz, $CDCl_3$): δ = 31.03 ppm. ^{13}C NMR (125 MHz, $CDCl_3$): δ = 147.82, 138.24, 134.31, 133.93, 129.12, 128.87, 125.83, 125.51, 124.52, 112.73, 53.77, 47.47, 26.51, 9.21 ppm. ^{29}Si NMR (99.32 MHz, $CDCl_3$): δ = –42.9 ppm (Figure S1). FTIR (KBr): $\tilde{\nu}_{max}$ = 1194, 1115 cm^{-1}.

Synthesis of Silylated Eu^{3+} Complex $[Eu(L2)_3$(Si-DPOXPO)]: The solvated Eu^{3+} complex $[Eu(\mathbf{L2})_3(C_2H_5OH)_2]$ (2 mmol) was dissolved in chloroform (20 mL). **Si-DPOXPO** (2 mmol) was added to the solution, and the mixture was stirred at 65 °C for 12 h. The solvent was then removed under reduced pressure. The product obtained was then washed with hexane, dried in vacuo, and used without further purification.

Synthesis of Nanoparticles: The amine-functionalized luminescent silica nanoparticles were synthesized by a water-in-oil reverse microemulsion in a one-pot synthesis procedure (Scheme 4). A water-in-oil reverse microemulsion was prepared by mixing cyclohexane (7.5 mL), octanol (1.82 mL), Triton X-100 (1.78 mL), and water (500 µL) and stirred for 15 min. The compound $[Eu(\mathbf{L2})_3$(**Si-DPOXPO**)] (4 mg) in toluene (1.5 mL) was added, and the mixture was stirred for 30 min (addition of a greater amount of complex may decrease the luminescence intensity by concentration quenching).[27] TEOS (100 µL) was added to this as a precursor for silica-shell formation, followed by aqueous ammonia (75 µL) to catalyze the hydrolysis and condensation of TEOS. For amine functionalization, APTES (10 µL) was added to the reaction mixture, which was stirred at room temperature for 24 h. The nanoparticles were then isolated by breaking the microemulsion with the addition of ethanol (4 mL). The prepared nanoparticles were separated by centrifugation, washed with a 1:2 mixture of ethanol/water and then with water to remove the surfactants and unreacted Eu^{3+} complexes. The washing was continued and tested with luminescence measurements until the washings exhibited no emission from unreacted $[Eu(\mathbf{L2})_3$(**Si-DPOXPO**)]. The synthesized nanoparticles **Eu@Si-NH2** and **Eu@Si-OH** were then characterized using Fourier transform infrared spectroscopy (FTIR), dynamic light scattering (DLS) spectrometry, transmission electron microscopy (TEM), and energy dispersive X-ray spectroscopy.

Cell-Imaging Experiments and Analyses: The cellular uptake was measured by transmission light microscopy and fluorescence microscopy with a Keyence Biorevo BZ-9000 instrument (Osaka, Japan). Confocal-laser-scanning microscopy was performed with a confocal-laser-scanning microscope (SP5 LCSM, Leica) using a 63× water objective. HeLa cells were cultured in Dulbecco's modified Eagle's medium (DMEM), supplemented with fetal calf serum (FCS, 10 %), streptomycin (100 U mL^{-1}), and penicillin (100 U mL^{-1}), at 37 °C under 5 % CO_2 atmosphere. **Eu@Si-NH2** nanoparticles were redispersed in autoclaved water at 0.25 mg mL^{-1} by sonication at 80 % amplitude and 0.8 pulse with sonotrode MS7 (Hielscher UP50 H) for 1 min. The particles were then diluted with DMEM [cell-culture medium, supplemented with fetal calf serum (10 %), streptomycin (100 U mL^{-1}), and penicillin (100 U mL^{-1})] to a concentration of 0.1 mg mL^{-1}. For CLSM, cells were seeded 1 d prior to the experiment at 10^5 cells/well in a four-chamber polystyrene tissue-culture-treated glass slide. The cells were incubated with the nanoparticle dispersion (excitation: 380 nm; emission: 612 nm). Afterwards, the cells were washed three times with PBS (phosphate-buffered saline) and incubated with formaldehyde (3.7 %) for fixation for 20 min. The cells were washed again two times with PBS before incubation with CellMask® (plasma membrane stain, Life Technologies, Carlsbad, USA; excitation: 649 nm; emission: 666 nm) to stain the cellular membrane. Afterwards, the cells were washed three times with PBS and stored overnight in mounting medium before microscopy.

MTT Assay (Cytotoxicity): The cell viability was analyzed by the MTT assay. Here, the enzyme mitochondrial dehydrogenase cleaved the tetrazolium ring of MTT and the pale-yellow solution became

dark-blue, because of the formation of formazan within the living cells. Only active mitochondria contain the enzyme mitochondrial dehydrogenase. For the MTT assay, the HeLa cells were seeded in 24-well plates with 5×10^4 cells per well. MTT [3-(4,5-dimethylthiazol-2-yl)-2,5-diphenyltetrazolium bromide; Molecular Probes, Life Technologies, Carlsbad, USA] was dissolved in PBS (5 mg mL^{-1}) and then added to the required amount of cell-culture medium to give a final MTT concentration of 1 mg mL^{-1}. The cell-culture medium of the cells was replaced by the MTT medium (300 µL) and incubated at 37 °C under 5 % CO_2 in a humidified atmosphere for 90 min. Then, the MTT medium was removed, and the blue precipitate was dissolved in DMSO (300 µL, each well) and incubated for 30 min. Finally, 100 µL of each well were taken for photometric analysis at λ = 570 nm (Multiscan FC instrument, ThermoFisher Scientific, Vantaa, Finland). The absorption of the supernatant of the cells treated with the nanoparticles was normalized to that of the control. In all cases, cells cultivated under the same conditions, but without any treatment, were used as the control.

Acknowledgments

B. F. thanks the Council of Scientific and Industrial Research (CSIR) and the Deutscher Akademischer Austauschdienst (DAAD) for fellowships. We thank Dr. Juri Barthel and the Gemeinschaftslabor für Elektronenmikroskopie RWTH-Aachen, Ernst-Ruska-Centrum für Mikroskopie, Spektroskopie mit Elektronen, FZ Jülich, Germany for TEM analysis.

Keywords: Europium · Biosensors · Luminescence · Cell uptake · Nanoparticles

[1] J. A. Thomas, *Chem. Soc. Rev.* **2015**, *44*, 4494–4500.
[2] Y. Liu, D. Tu, H. Zhu, E. Ma, X. Chen, *Nanoscale* **2013**, *5*, 1369–1384.
[3] M. Schäferling, *Angew. Chem. Int. Ed.* **2012**, *51*, 3532–3554; *Angew. Chem.* **2012**, *124*, 3590.
[4] S. V. Eliseeva, J.-C. G. Bunzli, *Chem. Soc. Rev.* **2010**, *39*, 189–227.
[5] C. Bouzigues, T. Gacoin, A. Alexandrou, *ACS Nano* **2011**, *5*, 8488–8505.
[6] U. Resch-Genger, M. Grabolle, S. Cavaliere-Jaricot, R. Nitschke, T. Nann, *Nat. Methods* **2008**, *5*, 763–775.
[7] X. Michalet, F. F. Pinaud, L. A. Bentolila, J. M. Tsay, S. Doose, J. J. Li, G. Sundaresan, A. M. Wu, S. S. Gambhir, S. Weiss, *Science* **2005**, *307*, 538–544.
[8] I. L. Medintz, H. T. Uyeda, E. R. Goldman, H. Mattoussi, *Nat. Mater.* **2005**, *4*, 435–446.
[9] O. S. Wolfbeis, *Chem. Soc. Rev.* **2015**, *44*, 4743–4768.
[10] P. Calero, R. Martínez-Máñez, F. Sancenón, J. Soto, *Eur. J. Inorg. Chem.* **2008**, 5649–5658.
[11] A. Burns, H. Ow, U. Wiesner, *Chem. Soc. Rev.* **2006**, *35*, 1028–1042.
[12] S. Bonacchi, D. Genovese, R. Juris, M. Montalti, L. Prodi, E. Rampazzo, N. Zaccheroni, *Angew. Chem. Int. Ed.* **2011**, *50*, 4056–4066; *Angew. Chem.* **2011**, *123*, 4142.
[13] S. Zanarini, E. Rampazzo, L. D. Ciana, M. Marcaccio, E. Marzocchi, M. Montalti, F. Paolucci, L. Prodi, *J. Am. Chem. Soc.* **2009**, *131*, 2260–2267.
[14] H. Ow, D. R. Larson, M. Srivastava, B. A. Baird, W. W. Webb, U. Wiesner, *Nano Lett.* **2005**, *5*, 113–117.
[15] L. Prodi, E. Rampazzo, F. Rastrelli, A. Speghini, N. Zaccheroni, *Chem. Soc. Rev.* **2015**, *44*, 4922–4952.
[16] N. Wartenberg, O. Raccurt, E. Bourgeat-Lami, D. Imbert, M. Mazzanti, *Eur. J. Inorg. Chem.* **2013**, 1493–1498.
[17] C. S. Neves, C. M. Granadeiro, L. Cunha-Silva, D. Ananias, S. Gago, G. Feio, P. A. Carvalho, P. Eaton, S. S. Balula, E. Pereira, *Eur. J. Inorg. Chem.* **2013**, 2877–2886.
[18] S. L. C. Pinho, H. Faneca, C. F. G. C. Geraldes, M.-H. Delville, L. D. Carlos, J. Rocha, *Biomaterials* **2012**, *33*, 925–935.
[19] M. C. Heffern, L. M. Matosziuk, T. J. Meade, *Chem. Rev.* **2014**, *114*, 4496–4539.
[20] H. Dong, S.-R. Du, X.-Y. Zheng, G.-M. Lyu, L.-D. Sun, L.-D. Li, P.-Z. Zhang, C. Zhang, C.-H. Yan, *Chem. Rev.* **2015**, *115*, 10725–10815.
[21] A. J. Amoroso, S. J. A. Pope, *Chem. Soc. Rev.* **2015**, *44*, 4723–4742.
[22] C. P. Montgomery, B. S. Murray, E. J. New, R. Pal, D. Parker, *Acc. Chem. Res.* **2009**, *42*, 925–937.
[23] T. V. Usha Gangan, M. L. P. Reddy, *Dalton Trans.* **2015**, *44*, 15924–15937.
[24] M. L. P. Reddy, V. Divya, R. Pavithran, *Dalton Trans.* **2013**, *42*, 15249–15262.
[25] S. Biju, L.-J. Xu, M. A. Hora Alves, R. O. Freire, Z.-N. Chen, *New J. Chem.* **2017**, *41*, 1687–1695.
[26] M. M. Unterlass, *Eur. J. Inorg. Chem.* **2016**, 1135–1156.
[27] L. Tian, Z. Dai, L. Zhang, R. Zhang, Z. Ye, J. Wu, D. Jin, J. Yuan, *Nanoscale* **2012**, *4*, 3551–3557.
[28] C. Gaillard, P. Adumeau, J.-L. Canet, A. Gautier, D. Boyer, C. Beaudoin, C. Hesling, L. Morel, R. Mahiou, *J. Mater. Chem. B* **2013**, *1*, 4306–4312.
[29] J. Wu, G. Wang, D. Jin, J. Yuan, Y. Guan, J. Piper, *Chem. Commun.* **2008**, 365–367.
[30] Y. Wu, M. Shi, L. Zhao, W. Feng, F. Li, C. Huang, *Biomaterials* **2014**, *35*, 5830–5839.
[31] J. Wu, Z. Ye, G. Wang, D. Jin, J. Yuan, Y. Guan, J. Piper, *J. Mater. Chem.* **2009**, *19*, 1258–1264.
[32] R. Kumar, I. Roy, T. Y. Ohulchanskyy, L. N. Goswami, A. C. Bonoiu, E. J. Bergey, K. M. Tramposch, A. Maitra, P. N. Prasad, *ACS Nano* **2008**, *2*, 449–456.
[33] L. D. Carlos, R. A. S. Ferreira, V. d. Z. Bermudez, S. J. L. Ribeiro, *Adv. Mater.* **2009**, *21*, 509–534.
[34] Z. Wang, X. Hong, S. Zong, C. Tang, Y. Cui, Q. Zheng, *Sci. Rep.* **2015**, *5*, 12602–12611.
[35] K. Binnemans, *Chem. Rev.* **2009**, *109*, 4283–4374.
[36] B. Francis, D. B. Ambili Raj, M. L. P. Reddy, *Dalton Trans.* **2010**, *39*, 8084–8092.
[37] A. P. Duarte, M. Gressier, M.-J. Menu, J. Dexpert-Ghys, J. M. A. Caiut, S. J. L. Ribeiro, *J. Phys. Chem. C* **2012**, *116*, 505–515.
[38] D. B. Ambili Raj, S. Biju, M. L. P. Reddy, *J. Mater. Chem.* **2009**, *19*, 7976–7983.
[39] A.-C. Franville, D. Zambon, R. Mahiou, Y. Troin, *Chem. Mater.* **2000**, *12*, 428–435.
[40] H. R. Li, J. Lin, H. J. Zhang, L. S. Fu, Q. G. Meng, S. B. Wang, *Chem. Mater.* **2002**, *14*, 3651–3655.
[41] K. Binnemans, P. Lenaerts, K. Driesen, C. Gorller-Walrand, *J. Mater. Chem.* **2004**, *14*, 191–195.
[42] H. Xu, K. Yin, W. Huang, *Chem. Eur. J.* **2007**, *13*, 10281–10293.
[43] H. Xu, K. Yin, W. Huang, *ChemPhysChem* **2008**, *9*, 1752–1760.
[44] H. Xu, L.-H. Wang, X.-H. Zhu, K. Yin, G.-Y. Zhong, X.-Y. Hou, W. Huang, *J. Phys. Chem. B* **2006**, *110*, 3023–3029.
[45] L. J. Charbonnière, R. Ziessel, M. Montalti, L. Prodi, N. Zaccheroni, C. Boehme, G. Wipff, *J. Am. Chem. Soc.* **2002**, *124*, 7779–7788.
[46] R. J. P. Corriu, F. Embert, Y. Guari, A. Mehdi, C. Reye, *Chem. Commun.* **2001**, 1116–1117.
[47] F. Embert, A. Mehdi, C. Reyé, R. J. P. Corriu, *Chem. Mater.* **2001**, *13*, 4542–4549.
[48] B. Francis, C. Heering, R. O. Freire, M. L. P. Reddy, C. Janiak, *RSC Adv.* **2015**, *5*, 90720–90730.
[49] L. Wang, W. Zhao, W. Tan, *Nano Res.* **2008**, *1*, 99–115.
[50] L.-F. Alejandro, D. Tristan, D. Silvio, S. Frank, J. M. Artur, J. M. Gerhard, *Nanotechnology* **2011**, *22*, 415501.
[51] E. Kaiser, R. L. Colescott, C. D. Bossinger, P. I. Cook, *Anal. Biochem.* **1970**, *34*, 595–598.
[52] J. A. Smith, *Anal. Biochem.* **1976**, *74*, 477–483.
[53] P. He, H. H. Wang, H. G. Yan, W. Hu, J. X. Shi, M. L. Gong, *Dalton Trans.* **2010**, *39*, 8919–8924.
[54] D. B. A. Raj, B. Francis, M. L. P. Reddy, R. R. Butorac, V. M. Lynch, A. H. Cowley, *Inorg. Chem.* **2010**, *49*, 9055–9063.
[55] G. F. de Sá, O. L. Malta, C. de Mello Donegá, A. M. Simas, R. L. Longo, P. A. Santa-Cruz, E. F. da Silva Jr., *Coord. Chem. Rev.* **2000**, *196*, 165–195.
[56] S. V. Eliseeva, B. Song, C. D. B. Vandevyver, A.-S. Chauvin, J. B. Wacker, J.-C. G. Bunzli, *New J. Chem.* **2010**, *34*, 2915–2921.

[57] S. J. Butler, M. Delbianco, L. Lamarque, B. K. McMahon, E. R. Neil, R. Pal, D. Parker, J. W. Walton, J. M. Zwier, *Dalton Trans.* **2015**, *44*, 4791–4803.
[58] K. Binnemans, *Coord. Chem. Rev.* **2015**, *295*, 1–45.
[59] B. Makhinson, A. K. Duncan, A. R. Elam, A. de Bettencourt-Dias, C. D. Medley, J. E. Smith, E. J. Werner, *Inorg. Chem.* **2013**, *52*, 6311–6318.
[60] J.-C. G. Bünzli, *Coord. Chem. Rev.* **2015**, *293–294*, 19–47.
[61] M. M. Nolasco, P. M. Vaz, V. T. Freitas, P. P. Lima, P. S. Andre, R. A. S. Ferreira, P. D. Vaz, P. Ribeiro-Claro, L. D. Carlos, *J. Mater. Chem. A* **2013**, *1*, 7339–7350.
[62] T. M. George, M. J. Sajan, N. Gopakumar, M. L. P. Reddy, *J. Photochem. Photobiol. A* **2016**, *317*, 88–99.
[63] N. Lewinski, V. Colvin, R. Drezek, *Small* **2008**, *4*, 26–49.
[64] L. Porrès, A. Holland, L.-O. Pålsson, A. Monkman, C. Kemp, A. Beeby, *J. Fluoresc.* **2006**, *16*, 267–273.
[65] J. C. de Mello, H. F. Wittmann, R. H. Friend, *Adv. Mater.* **1997**, *9*, 230–232.
[66] L. O. Pålsson, A. P. Monkman, *Adv. Mater.* **2002**, *14*, 757–758.
[67] N. S. S. Kumar, S. Varghese, N. P. Rath, S. Das, *J. Phys. Chem. C* **2008**, *112*, 8429–8437.
[68] M. Cölle, J. Gmeiner, W. Milius, H. Hillebrecht, W. Brütting, *Adv. Funct. Mater.* **2003**, *13*, 108–112.
[69] S. V. Eliseeva, O. V. Kotova, F. Gumy, S. N. Semenov, V. G. Kessler, L. S. Lepnev, J.-C. G. Bünzli, N. P. Kuzmina, *J. Phys. Chem. A* **2008**, *112*, 3614–3626.
[70] M. S. Wrighton, D. S. Ginley, D. L. Morse, *J. Phys. Chem.* **1974**, *78*, 2229–2233.

Received: March 5, 2017

